The small-scale turbulent structure of the high latitude ionosphere - Arcad-Aureol-3 observations

H. Mounir, Jean-Jacques Berthelier, J. C. Cerisier, Dominique Lagoutte, Christian Béghin

Ann. Geophysicae 9, 725–737 (1991)

Annales Geophysicae

The small-scale turbulent structure of the high latitude ionosphere: ARCAD-AUREOL-3 observations

H. Mounir [1], J. C. Cerisier [1,3], A. Berthelier [1], D. Lagoutte [2], and C. Beghin [2]

[1] Centre de Recherches en Physique de l'Environnement, 4 Avenue de Neptune, F-94107 Saint-Maur-des-Fossés Cedex, France
[2] Laboratoire de Physique et Chimie de l'Environnement, 3A, Avenue de la Recherche Scientifique, La Source, F-45071 Orléans Cedex 2, France
[3] Université Pierre et Marie Curie, 4 Place Jussien, F-75252 Paris, Cedex

Received April 23, 1991; revised August 7, 1991; accepted October 7, 1991

Abstract. Electric field and electron density measurements made by the Arcad-Aureol-3 satellite are used to study the small scale structure of the high latitude topside ionosphere. The frequency range is between 12.5 and 200 Hz, which, under the hypothesis of zero frequency turbulence, corresponds to spatial wavelengths between 40 m and 640 m. Two different groups of regions have been identified, in which different types of turbulence are observed: (1) the arc region of the auroral zone, where intense sporadic turbulence events occur ($E = 1$ mV/m rms), which are associated with precipitations, parallel current and velocity shears; (2) the polar cap, diffuse auroral zone and sub auroral region, where the turbulence is less intense ($E = 0.1$ mV/m rms) and often associated with density gradients. This second type, called gradient-drift turbulence has been associated to the generalized $\mathbf{E} \times \mathbf{B}$ instability. The frequency spectra of the electric and density fluctuations generally have a power law shape (power $\propto f^{-\alpha}$). The distribution of the spectral indices, α, is different in each type of turbulence, with smaller and less dispersed values in the $\mathbf{E} \times \mathbf{B}$ turbulence than in shear-associated turbulence. The most important differences between these two types of turbulence are the existence of magnetic fluctuations in shear-associated turbulence and the value of the ratio of the electric field to the density fluctuations. This ratio is larger by a factor of 10–100 in the shear-associated turbulence compared to the gradient-drift turbulence.

Introduction

The high latitude ionosphere contains irregularities in the plasma structure with spatial scales ranging from hundreds of kilometers down to a few meters, corresponding to the gyroradius of thermal ions. General reviews of observations and theories have been made recently by Kintner and Seyler (1985), Tsunoda (1988) and Kelley (1989). Initially, the turbulent structure of the ionosphere has been deduced from density measurements for the larger scales and from electric measurements (Kelley and Mozer, 1972; Kintner, 1976) for the smaller scales. The existence of small scale turbulence has also been deduced from the observation of scintillations in the transmission of HF signals. Only a few recent experiments have simultaneously measured the electric and density fluctuations (Cerisier *et al.*, 1985; Basu *et al.*, 1988, 1990).

Several mechanisms have been proposed to generate the small scale plasma turbulence in the high latitude F-region. The larger scale irregularities ($\lambda > 10$ km), also called blobs, are believed to be created by particle precipitations (Kelley *et al.*, 1982) or to result from turbulent mixing or from plasma detached from the denser low latitude plasma regions by a rapidly changing convection pattern. These blobs are a source of density gradients transverse to the earth magnetic field. Experimentally, they have been identified as the place where smaller scale (from hundreds of meters to 10 km) irregularities develop through non-linear cascading processes towards smaller wavelengths. These observations have led to the hypothesis that interchange processes such as the gradient drift and current convective instabilities play a major role in structuring the high latitude plasma (Keskinen and Ossakow, 1983 a). This gradient drift turbulence has been observed at all latitudes above the plasmapause, from subauroral regions to the polar cap.

In addition to the turbulent mixing process, the inhomogeneity of the plasma flow is a potential source of free energy which can drive the Kelvin-Helmholtz instability. Shears in the transverse convection are often observed in association with auroral arcs and with gradients in the parallel current and in the parallel velocity. Increase events of turbulence have been shown to occur in these regions, initially by Kintner (1976) and, later, by Berthelier *et al.* (1988) and by Basu *et al.* (1988).

Offprint requests to: J. C. Cerisier

The frequency spectra of the turbulence are usually well fitted by power laws. Power law spectra, but in k-space, are also obtained by numerical simulations of a two-dimensional turbulence, both in the gradient drift case (Keskinen and Ossakow, 1982, 1983a) and in the Kelvin-Helmholtz case (Keskinen *et al.*, 1988). Experimentally, several authors have shown that electric low frequency fluctuations observed in the satellite frame at ionospheric altitudes (Kelley and Mozer, 1972) and also higher along auroral field lines (Temerin, 1978; Holmgren and Kintner, 1990) are Doppler shifted spatial fluctuations. It is then possible to compare the spectral indices of the frequency spectra with those of the one-dimensional wave-number spectra (Fredricks and Coroniti, 1976). Such comparisons have been made by Basu *et al.* (1988) who showed that there is a good agreement between simulations of the Kelvin-Helmholtz instability and turbulence associated with moderate shears.

The large range of wavelengths involved and the numerous available free energy sources make it clear that there is no unique physical process responsible for the turbulence. It is thus important to distinguish experimentally between different types of turbulence events and to establish their characteristics, such as the amplitude and the spectral index of the electric and density fluctuations and the relation between the occurrence of the turbulence and the electrodynamic parameters of the medium. In this paper, we describe the characteristics of the turbulence observed by the Arcad-Aureol-3 satellite (hereafter called A-3) in the upper ionosphere at high latitudes, in the frequency range 12.5–200 Hz, which, under the hypothesis of zero-frequency turbulence, corresponds roughly to wavelengths between 40 m and 640 m. From measurements of the electric field and electron density, we deduce the amplitude and power spectra of the fluctuations and we study their relation with the available free energy sources in the plasma. It is shown that turbulence of the gradient drift type is observed throughout the polar cap, auroral and subauroral regions, whereas stronger events, associated with shears in the convection of the plasma, are observed in the auroral and cusp regions, and that these two types of turbulence have different characteristics. In addition to a steeper power spectrum for shear-associated turbulence than for the gradient-drift turbulence, the electric field fluctuations are typically between one and two orders of magnitude larger in shear-driven turbulence while the density fluctuations remain at the same level in the two types of turbulence. Also, magnetic fluctuations are observed in association with shear-associated turbulence. These results are compared with those obtained by other spacecraft experiments (Basu *et al.*, 1988, 1990) and also with results of numerical simulation (Keskinen and Ossakow, 1983b; Huba *et al.*, 1988; Keskinen and Huba, 1990).

Instrumentation and data presentation

The A-3 spacecraft was built in the frame of the French-Soviet cooperation and launched on a low altitude (400–2000 km) polar orbit. To understand this paper, it is sufficient to know that the satellite is a three-axis gravity gradient stabilized spacecraft, with the z-axis along the local vertical and the x-axis in the orbital plane, the orientation of these axes being maintained within less than 15° from their nominal orientation. The wave experiment (Berthelier *et al.*, 1982a), consists of three magnetic and two electric channels. The two components of the electric field are E_Z along the z axis and E_H in a direction approximately in the x-y plane and tilted at 15° from the y direction. Thus, at high latitudes, the E_Z electric antenna is close to the earth magnetic field direction and the E_H antenna is approximately perpendicular both to the orbital velocity and to the static magnetic field. Each electric antenna consists of two spherical probes at the ends of booms, the length of which is 7.43 m for E_H and 2.36 m for E_Z. The frequency range is 10 Hz–1500 Hz for all 5 channels and the signals are telemetered to the ground in real time. DC electric and magnetic fields are also measured with sampling rates between 1 and 12.5 points/s (Berthelier *et al.*, 1982b).

The electron density is measured by a mutual impedance probe (Beghin *et al.*, 1982). Density measurements with a high time resolution (1 ms) are made when the probe is operated in the self oscillating mode, in which the sounding frequency is controlled by the resonance frequency of the plasma. This is possible only when the resonance spike at the upper hybrid frequency is sharp, a situation which needs a large enough electron density ($N_e > 10^4$ cm^{-3}). This explains why the orbits discussed in this paper are at a relatively low altitude.

From the examination of a large number of orbits, a first classification of the turbulence events can be made according to their region of occurrence. Outside of the regions of precipitations and of field aligned currents, the main source of free energy is the convection drift of the density gradients and the turbulence is often clearly related to these gradients, suggesting a gradient drift origin of the turbulence. On the other hand, in the auroral region, where currents and precipitations often coexist, the characteristics of the turbulence are more complex and clear identification of a single source of free energy and of the linear instability mechanism initiating the development of the turbulence is more difficult. However, in regions where auroral arcs are observed, identified by structured precipitations and localized field-aligned currents, the turbulence is usually more intense and clearly correlated with shears in the convection velocity.

In order to examplify the characteristics of the turbulence, we mainly present in this paper detailed results of two orbits, taking advantage of other data when necessary. Their large-scale characteristics are shown on Figs. 1 and 2. Orbit 2314 (Fig. 1) is a morning pass from the polar cap through the auroral zone and towards subauroral latitudes. The auroral zone, which can be identified from the electron precipitation is crossed between 0447 and 0451 UT. A series of intensifications in the electron precipitation, probably associated with auroral arcs, are observed on the high latitude side of the auroral region, whereas on the low latitude side, the precipitations are more regular. Parallel currents, alternatively downgoing and upgoing, are observed between 0447 and

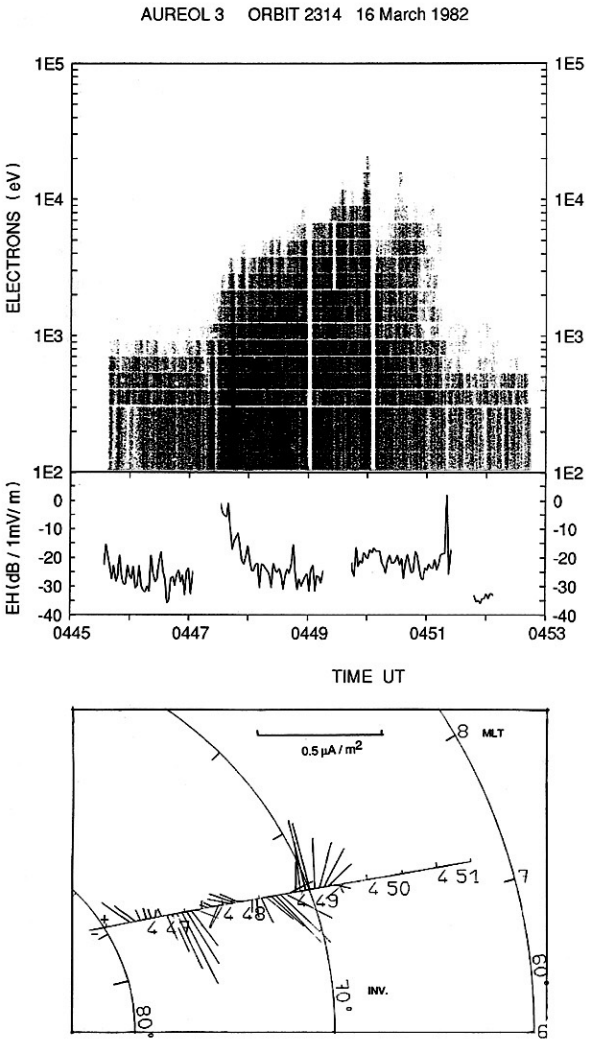

Fig. 1. Orbit 2314. From *top* to *bottom* are shown: the energy-time spectrogram of precipitated electrons; the rms electric field component E_H in the range 12.5–200 Hz; the situation of the orbit in an INV-MLT diagram. The direction of the lines drawn from the orbit represent the direction of the current sheets and their length is proportional to the intensity of the field-aligned current density. *Positive* (*negative*) values indicate *upward* (*downward*) field-aligned currents

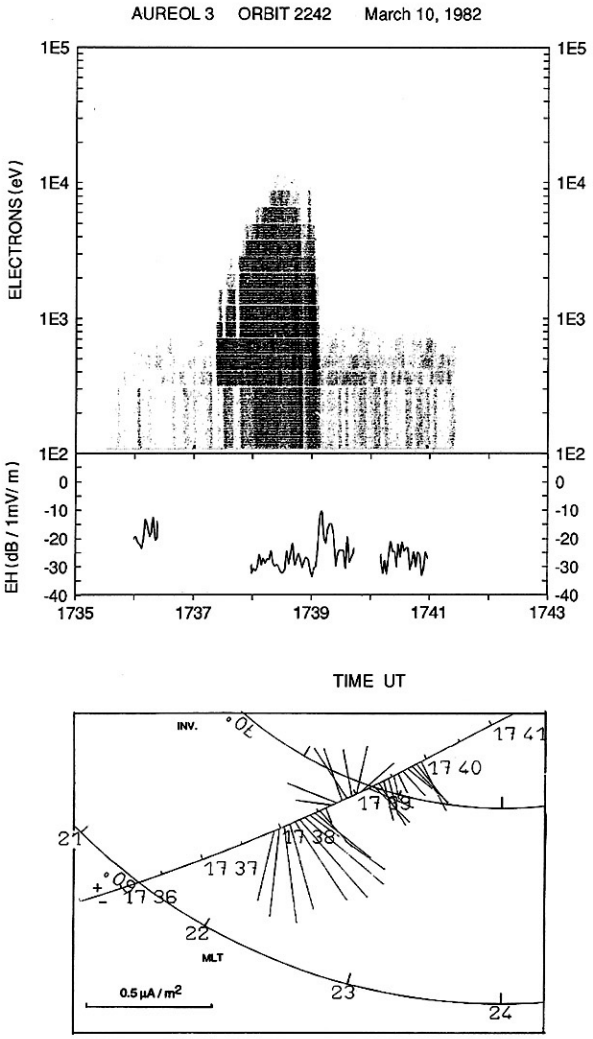

Fig. 2. Orbit 2242. From top to bottom are shown: the energy-time spectrogram of precipitated electrons; the rms electric field component E_H in the range 12.5–200 Hz; the situation of the orbit in an INV-MLT diagram. The direction of the lines drawn from the orbit represent the direction of the current sheets and their length is proportional to the intensity of the field-aligned current density. *Positive* (*negative*) values indicate *upward* (*downward*) field-aligned currents

0450 UT. The root mean square (rms) value of the E_H component of the electric field, integrated between 12.5 and 200 Hz shows fluctuations above the antenna noise level (which is about 38 dB below 1 mV/m). These spikes in the rms electric field are observed all over the polar cap, auroral and sub-auroral zones and indicate the existence of spatially inhomogeneous turbulence. Interruptions in the data are due to onboard calibrations of the electric sensors which occur every 128 s. The electric turbulence is more intense in the arc region than in the polar cap and in the diffuse aurora. The second orbit (orbit 2242, Fig. 2), which shows similar features, is a pass from auroral latitudes to the polar cap through the evening MLT sector. For these two orbits, the magnetic activity is low to moderate ($Km = 1^+ - 3^-$; AE < 100 nT). Both orbits are at relatively low altitude, between 400 km and 800 km.

Turbulence outside the auroral zone

Examples of the gradient drift turbulence

Figures 3 and 4 display several detailed examples of turbulence events observed at high latitude outside the auroral zone. On each of these figures, the different panels show the plasma frequency, the fluctuations of the elec-

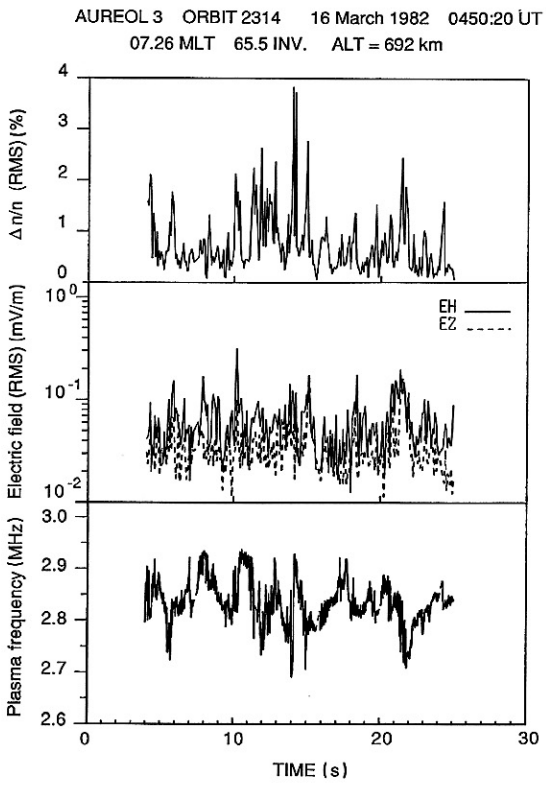

Fig. 3. Turbulence observed at sub-auroral latitudes during orbit 2314. From top to bottom are displayed: the rms fluctuation of the relative density in the range 12.5–200 Hz; the electric field fluctuation in the same frequency range; the plasma frequency

tron density and the ELF electric field components E_H and E_Z. These fluctuations are rms values, integrated between 12.5 and 200 Hz. The lower frequency limit is imposed by the cut-off frequency of the VLF experiment. The upper limit of 200 Hz has been chosen in order to avoid the contamination of the signal by electromagnetic waves such as ELF hiss which is a common feature above 200 Hz in these altitude and latitude ranges. In addition, the variations of the electron density gradient along the orbit are shown on Fig. 4a, b.

Figure 3 from orbit 2314 shows measurements made at sub-auroral latitudes. Figure 4a, also from orbit 2314, and Fig. 4b, from orbit 2242, illustrate results obtained in the polar cap. The clear association between density and electric field fluctuations is emphasized by vertical arrows. Figure 4a, b also gives spectacular evidence of increases in the turbulence level associated with positive density gradients of the blobs characteristic of the polar cap region. On the contrary, such a correlation is absent in the sub-auroral case of orbit 2314 shown on Fig. 3.

Relation between the amplitudes of E_H, E_Z and $\Delta N/N$

The relation between the rms amplitudes of the electric field components E_H and E_Z is illustrated on Fig. 5 for the polar cap data of the two orbits. As expected, it can be described by a linear relationship between these two components. In the case of orbit 2314, and for signal intensities larger than 30 μV/m, the E_H component is about 6 dB above the E_Z component, indicating that the turbulence is polarized in the plane perpendicular to the earth magnetic field, (recall that E_H is close to the perpendicular to the earth magnetic field, while E_Z is close to parallel). Notice that this linear relationship is not true for the lower values of the amplitude of the turbulence, where the E_Z component tends to have the same amplitude as the E_H component. This spurious effect is due to a larger noise level on E_Z. For orbit 2242, the two components have similar amplitudes, suggesting that the turbulence is quasi-isotropic. A thorough discussion of the anisotropy of the turbulence spectrum is planned to be the subject of a further paper.

The relationship between the fluctuations of the E_H electric field component and the density fluctuations is illustrated in Fig. 6. Although the data points are largely scattered through the diagram, it indicates that these two quantities are approximately proportional. The coefficient of proportionality between the amplitudes of the electric field and the relative density fluctuations can be estimated between 4 and 7 mV/m.

Power spectra

Power spectra of the two components E_H and E_Z of the electric field and of the electron density fluctuations are shown on Fig. 7. These spectra, from orbit 2314, have been calculated for the same time interval. In each spectrum, the intensity decreases regularly and the relationship between the energy density and the frequency can be approximated by a power law, characterized by the spectral index α which is defined as the slope of the spectrum in logarithmic coordinates ($P = A f^{-\alpha}$). In this example, the E_H field and the density have equal spectral indices whereas the E_Z field is characterized by a smaller value. Spectral indices of the two electric components and of the density have been calculated for about 40 events observed during orbits 2314 and 2242 outside the auroral zone. Their statistical distribution is given by the histograms of Fig. 8. Each spectral index is calculated over a time period of 1.2 s, which corresponds to 15 elementary spectra. Values of the indices smaller than 1.0 are not shown. The mean value of the spectral index is about 1.6 for the E_H electric component and for the density, and slightly less for the E_Z electric component. However, the width of the distribution of the indices is larger for the electron density than for the E_H electric field. In particular, it includes values larger than 2.2. Also, the values of the indices of the electric field and of the density are not correlated.

Auroral zone turbulence

Examples of auroral zone turbulence

In the auroral zone, the turbulence appears more complex than in the polar cap and sub-auroral zone. An

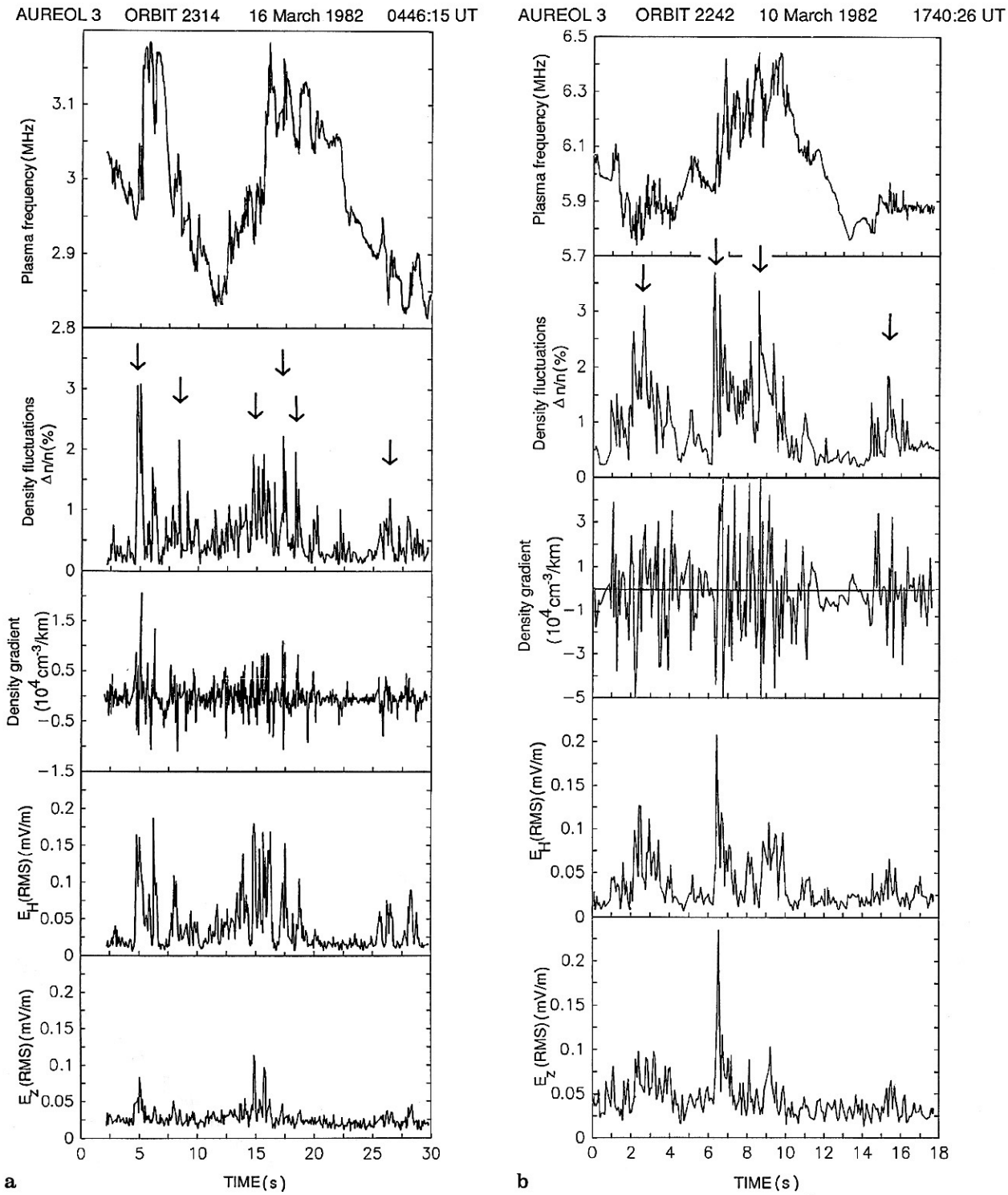

Fig. 4. **a** Turbulence observed in the polar cap during orbit 2314. From top to bottom are displayed: the plasma frequency; the rms fluctuation of the relative electron density in the range 12.5–200 Hz; the density gradient along the orbit; the electric field fluctuation E_H in the same frequency range; the electric field fluctuation E_Z in the same frequency range. **b** Turbulence observed in the polar cap during orbit 2242. From top to bottom are displayed: the plasma frequency; the rms fluctuation of the relative density in the range 12.5–200 Hz; the density gradient along the orbit; the electric field fluctuation E_H in the same frequency range; the electric field fluctuation E_Z in the same frequency range

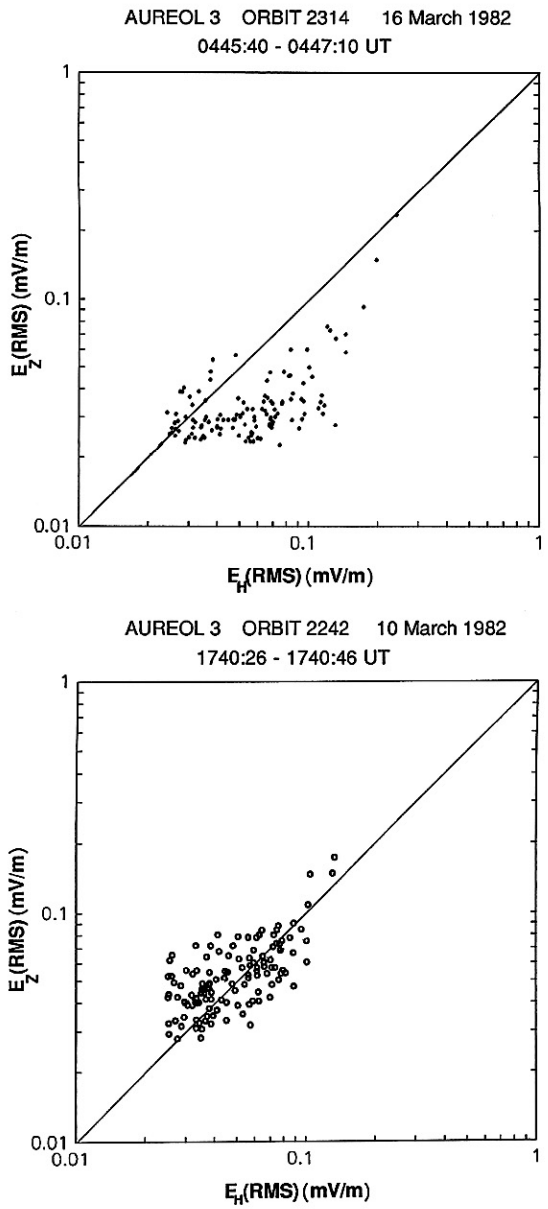

Fig. 5. Relation between the r.m.s. amplitudes of the electric components E_H and E_Z in the gradient drift turbulence: (*Top*) Orbit 2314; (*Bottom*) Orbit 2242

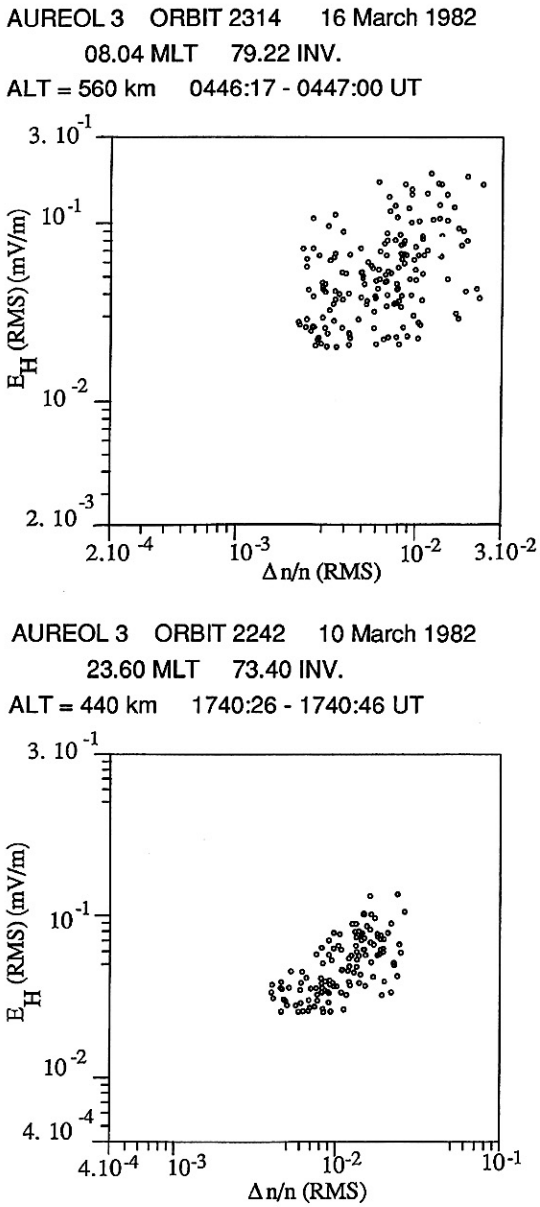

Fig. 6. Relation between the r.m.s. amplitudes of the electric component E_H and of the relative density fluctuation $\cdot\ \Delta N/N$: (*Top*) Orbit 2314; (*Bottom*) Orbit 2242

example is given in Fig. 9, which shows observations made during orbit 2314. From 0447:30 to 0447:40 UT, the satellite crosses a region of structured precipitation, characteristic of auroral arcs. In this region, the electric field turbulence is intense, with amplitudes as large as 1 mV/m rms. After 0477:40 UT, the satellite enters the diffuse auroral zone, where the electron flux is more steady and where the amplitude of the electric turbulence decreases down to the mean level of 0.1 mV/m rms. During these two periods, the density fluctuations remain at the same level, between 0.5 and a few percent rms, which means that the arc region is characterized by a larger value of the ratio of the electric field to the density fluctuations. This suggests that the nature of the turbulence is different in the arc region and in the diffuse auroral zone, a point which will be discussed in more detail below.

Characteristics of the turbulence in the diffuse auroral zone

Figure 10 shows the amplitudes of the electric field and electron density fluctuations during turbulence events observed in the diffuse auroral zone. These results are similar to those obtained for the turbulence observed outside

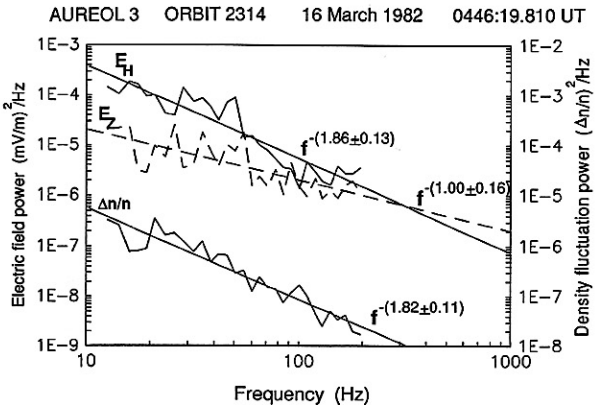

Fig. 7. Power spectra of the electric field components E_H and E_Z and of the relative density fluctuation $\cdot \Delta N/N$ in the gradient drift turbulence

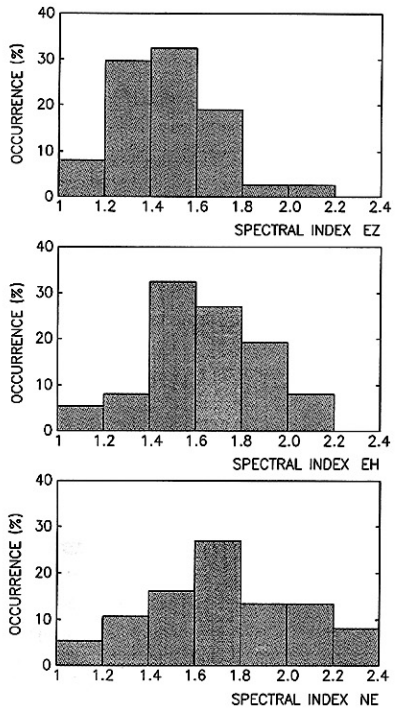

Fig. 8a–c. Histograms of the power spectral indices in the gradient drift turbulence. From top to bottom: **a** E_Z electric field; **b** E_H electric field; **c** the relative electron density

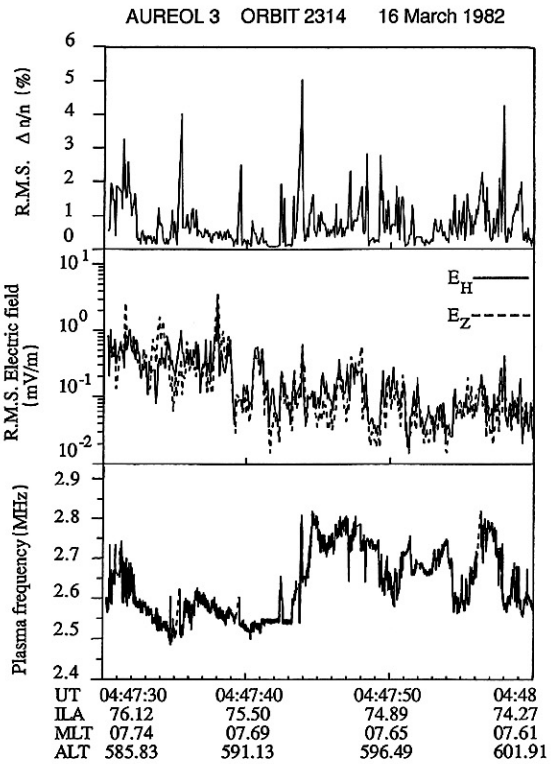

Fig. 9. Turbulence observed in the auroral zone. From top to bottom: the rms fluctuation of the relative density in the range 12.5–200 Hz; the electric field fluctuations E_H and E_Z in the same frequency range; the plasma frequency. The intensity of the turbulence is larger in the region of auroral arcs on the polar side of the auroral zone than on the low latitude side

of the auroral zone, except that the relative amplitude of the E_Z component of the electric field compared with that of the E_H component is larger. For a series of turbulence events observed during orbit 2314, the average value of the ratio of the intensities is $E_Z/E_H = 0.8$, compared with 0.4 for the turbulence observed outside of the auroral zone.

The power spectral indices have also been calculated for the same series of turbulence events. Histograms of the distribution of these indices for E_H, E_Z, and the density are shown on Fig. 11. As in the case of the turbulence observed in the polar cap and in the sub-auroral region, we observe a trend for the distribution of the spectral index of the density fluctuations to be more flat than the electric field distributions and to include larger values, up to 2.8. The mean value of each distribution is however slightly larger in the diffuse auroral zone than outside of the auroral zone by about 0.2 units. It must be mentioned also that there is no correlation between the values of the spectral index of the electric field and of the density.

Turbulence associated with auroral arcs and shears

Figure 12 shows an example of a shear-associated turbulence event observed at low altitude (430 km) in the midnight sector. Unfortunately, due to telemetry failure, only the E_y component of the DC electric field transverse to the satellite motion is available for that orbit. However, assuming that the direction of the convection velocity remains constant and parallel to the plane of the sheets of field-aligned currents, the intensity of velocity shears can be deduced from the variation of the E_y component of the electric field in the following way. The intensity of the

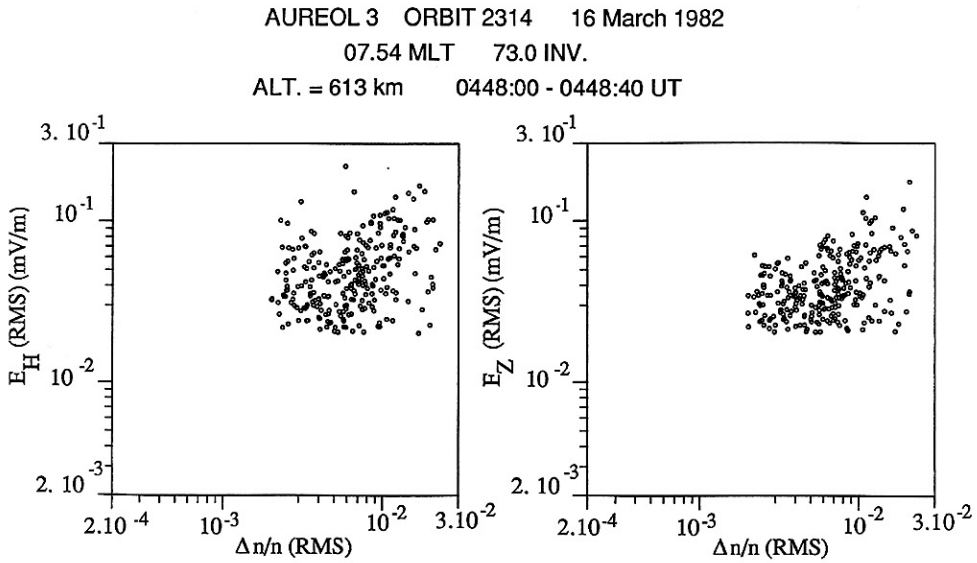

Fig. 10. Relation between the r.m.s. amplitudes of the electric components E_H (*right*) and E_Z (*left*) and the relative density fluctuation $\cdot \Delta N/N$ during orbit 2314. The data are obtained in the auroral zone, outside of the region of auroral arcs

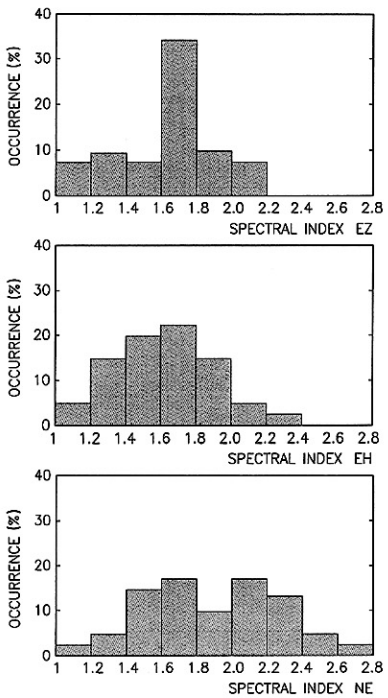

Fig. 11a–c. Histograms of the power spectral indices in the turbulence observed in the auroral zone outside of the region of auroral arcs. From top to bottom, **a** E_H electric field; **b** E_Z electric field; **c** the relative electron density

field-aligned currents and the direction of the current sheet are deduced from the DC magnetic fluctuations. From the ionospheric Ohm's law, the fluctuations of the magnetic field and the electric field are perpendicular (Sugiura *et al.*, 1982), so that the direction of the convection velocity (which is perpendicular to the electric field) is the same as that of the magnetic fluctuations. Then the shear intensity, defined as the derivative of the convection velocity in the direction perpendicular to it, is given by

$$C = \frac{1}{\sin\theta\cos\theta}\frac{dV_x}{dx} = \frac{1}{\sin\theta\cos\theta}\frac{1}{V_s B}\frac{dE_y}{dt}$$

where θ is the angle between the direction of the magnetic fluctuations and the orbit of the satellite, B is the Earth's magnetic field and V_s is the velocity of the satellite with respect to the plasma, supposed to be equal to the orbital velocity. It must be remarked that the above calculation is not valid when θ is either close to 0 or to $\pi/2$. The period illustrated on Fig. 12 is characterized by large variations of E_y, which are associated with a peak value of the shear intensity close to $4\,s^{-1}$. The electrodynamic parameters represented on Fig. 12 show a sharp increase during the period of strong shear. The parallel current shows small-scale structures (a few kilometers transverse to the Earth magnetic field) with intensities as large as $50\,\mu A/m^2$. The flux of precipitated electrons is increased by a factor 50 above the background level during the event, reaching a value of 8×10^9 $(cm^2\cdot s\cdot ster\cdot keV)^{-1}$ in the 750 eV channel. The intensity of the electric turbulence is increased by about 20 dB during the same period.

Figure 13 shows another example observed at a higher altitude (1782 km). The maximum values of the shear reaches $8\,s^{-1}$ and are associated with peaks in the amplitude of the electric component of 30 mV/m rms in E_H and more than 100 mV/m rms in E_Z. It must also be emphasized that, in agreement with previous observations (Kintner, 1976; Gurnett *et al.*, 1984; Berthelier *et al.*, 1988), these shear events are systematically characterized by simultaneous electric and magnetic fluctuations.

Further results concern the power spectra of the electric field and of the density fluctuations observed during

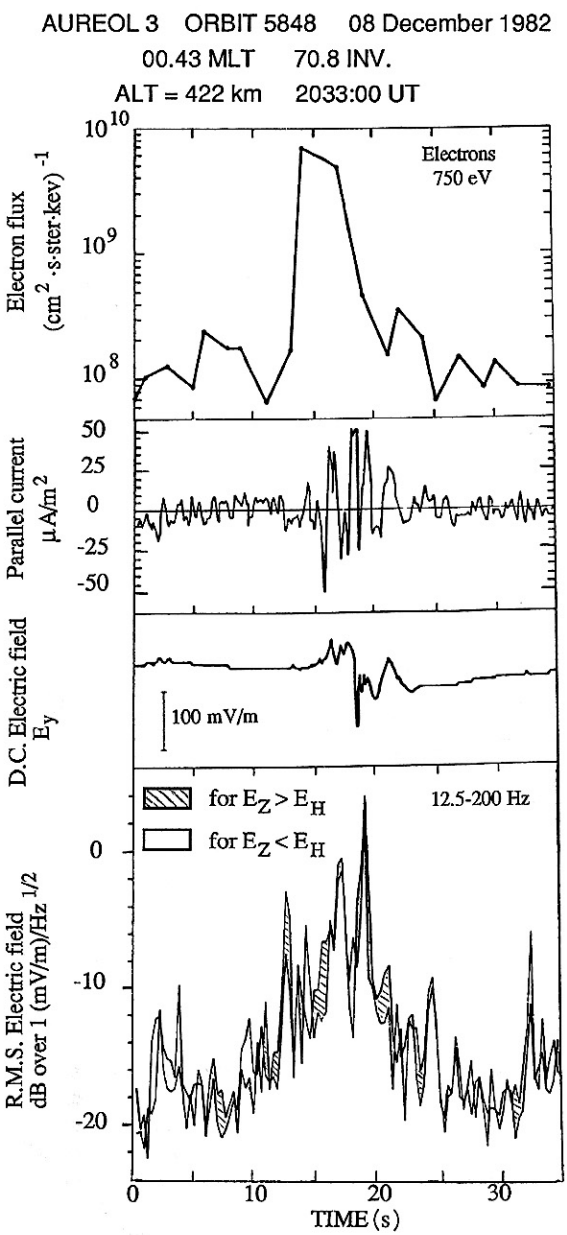

Fig. 12. Turbulence event associated with an auroral arc. From top to bottom are displayed: the downstream flux of electrons at 750 eV; the parallel current deduced from dc magnetometer measurements; the dc electric field component transverse to the orbit; the rms amplitudes of the electric components E_H and E_Z

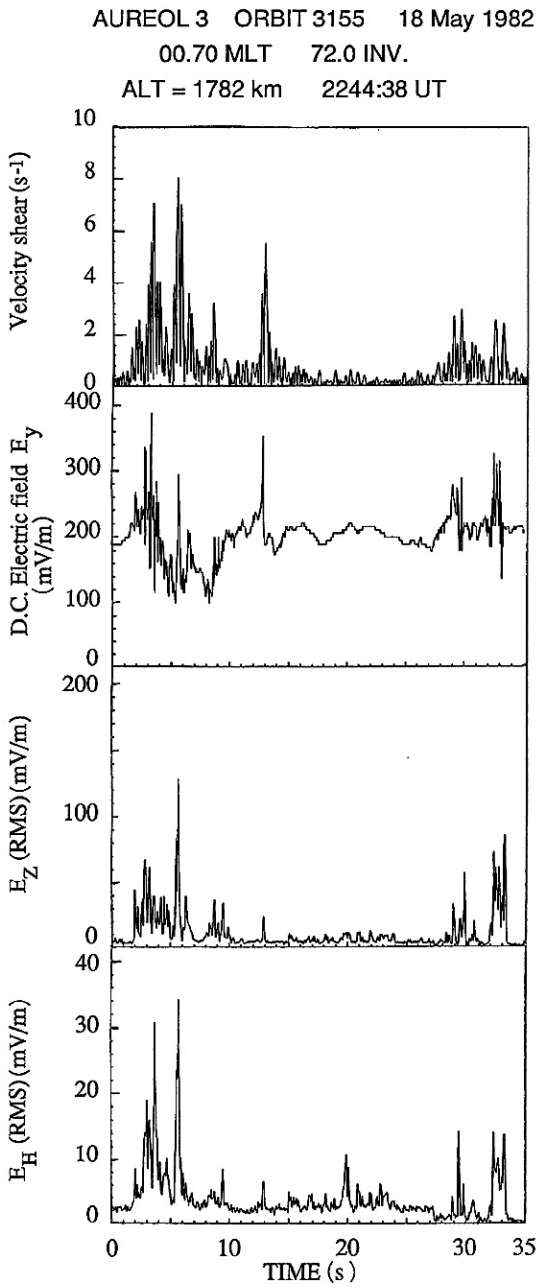

Fig. 13. Turbulence event associated with a shear in the convection velocity. From top to bottom are displayed: an evaluation of the shear intensity; the dc electric field component transverse to the orbit; the rms amplitude of the electric component E_Z. The rms amplitude of the electric components E_H

two turbulence events associated with shears, as shown on Fig. 14, for which the values of the shear intensity are different. Again these spectra can be described by power laws. Case a, which corresponds to a moderate shear ($C=0.6\ s^{-1}$), is characterized by a sharp electric field spectrum ($\alpha_H=3.13$), while case b, for which $C=1.4\ s^{-1}$ has a shallower electric field spectrum ($\alpha_H=1.66$). In both cases, the density spectrum has the same spectral index, $\alpha_N=1.72$. Histograms of the spectral indices of the electric and magnetic fluctuations representative of a set of about 50 shear events are shown on Fig. 15. The electric field indices are spread over a larger range of values than for the non-shear-associated turbulence. For the E_H component, the most probable value is between 1.6 and 1.8, although values up to 3.6 are observed. The indices for the E_Z component are larger than those of the transverse

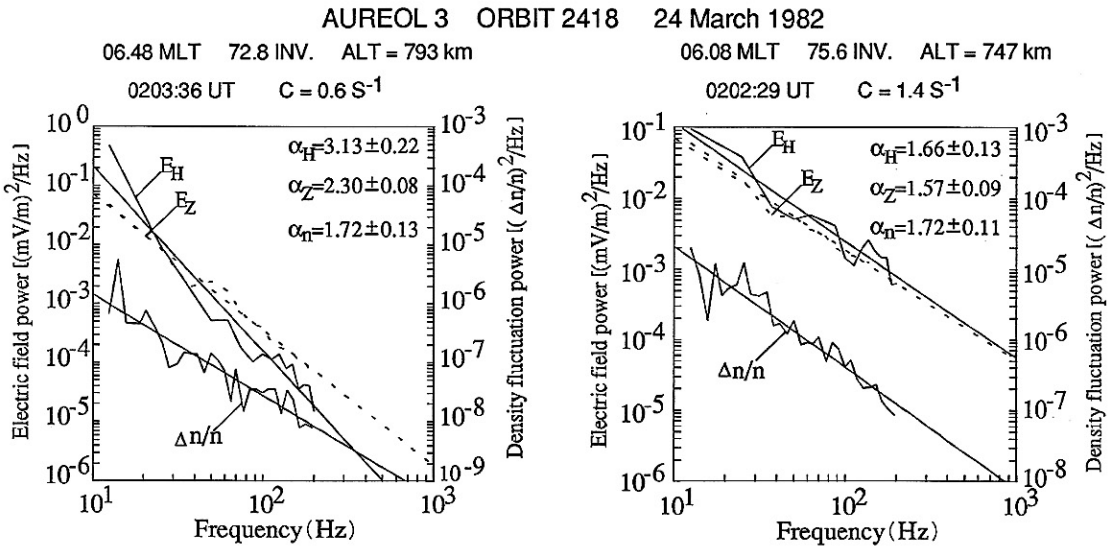

Fig. 14. Power spectra of the electric field components E_H and E_Z and of the relative density for two examples of shear associated turbulence. The shear intensity is: (*left*) 0.6 s^{-1}, (*right*) 1.4 s^{-1}

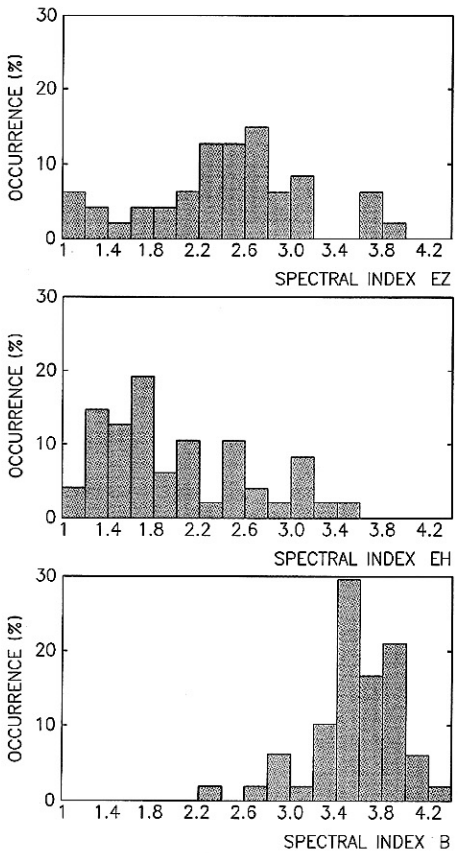

Fig. 15a–c. Histograms of the power spectral indices in shear associated turbulence. From top to bottom are displayed: **a** the E_H electric component; **b** the E_Z electric component; **c** the magnetic field component

component E_H and centered on 2.4. The spectral index of the magnetic power spectra are less dispersed and much larger than those of the electric field, with a mean value of 3.6.

Discussion

We will discuss the A-3 results by referring to existing instability theories and numerical simulations. Experimentally, we will refer to two papers by Basu *et al.* (1988, 1990), hereafter called paper 1 and paper 2, where results of high latitude turbulence measurements made by the Dynamic Explorer 2 (DE-2) satellite are presented. Paper 1 is devoted to shear-driven processes while paper 2 concerns the gradient-drift turbulence. Assuming that the fluctuations are frozen in the plasma frame (zero-frequency turbulence) and that the plasma convection velocity is smaller than the satellite velocity, the relation between wavelength and frequency is deduced simply from the Doppler shift due to the satellite motion. DE-2 results concern mainly wavelengths larger than ≈ 1 km and, to a smaller extent, small wavelengths ($\lambda < 125$ m). The wavelength range discussed in this paper is between 40 m and 640 m, intermediate between the two ranges studied by DE-2, although it overlaps slightly the short scale range. We will compare the A-3 measurements to the DE-2 results in order to emphasize their complementarity and their differences.

Spectral indices

The spectral indices obtained from A-3 measurements in the gradient drift turbulence (Fig. 8) are in the range

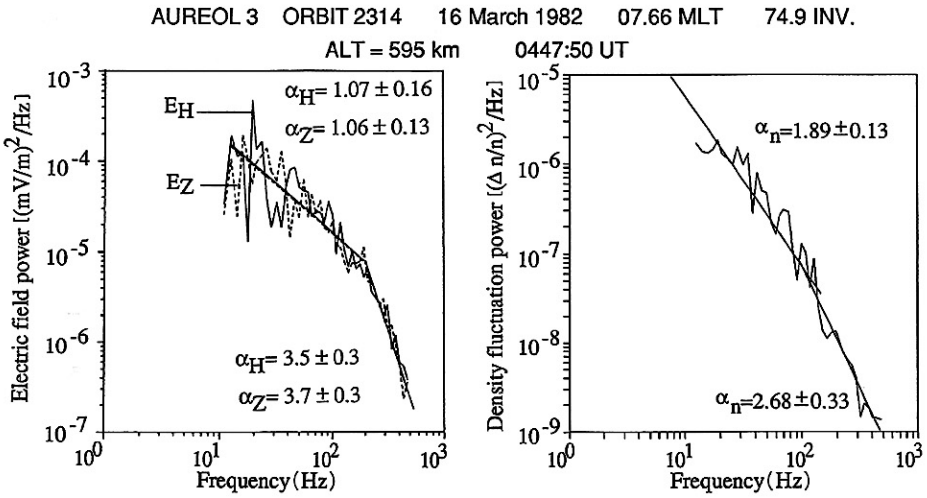

Fig. 16. Example of double power law spectra of the electric field (*left*) and electron density (*right*) observed in the auroral zone turbulence. The transition between the two values of the spectral index occurs at about 200 Hz (40 m wavelength) and corresponds to an increase in the slope of the spectra

1.6–1.8 for the wavelength interval between 40 m and 640 m. The majority of the values are between 1.4 and 1.6 for the electric field and between 1.6 and 1.8 for the electron density. These values are close to those obtained by DE-2 in the long wavelength range, where the mean value of the spectral index is equal to 1.8 ± 0.2 for both the electric field and the density fluctuations. This means that the spectral index remains quasi-constant (within about 0.2 unit) for wavelengths between 10 km and 40 m covered by DE-2 and A-3. At shorter wavelengths, it is shown in paper 2 that the density spectral slope increases to values between 2.5 and 3.5. This result is to be related to (and agrees with) the observation made on board A-3 of spectra which are better fitted by power laws with different indices in different frequency ranges (Villain *et al.*, 1986; Mounir, 1989; Tsunoda, private communication). An example of such an event is given in Fig. 16 for the electric and density fluctuations. For that example, the spectral analysis has been extended up to 500 Hz for both fields. The "knee" in the spectrum occurs at a frequency around 200 Hz (wavelength of 40 m) and corresponds, as it is always the case, to an increase in the slope at the higher frequencies. The wavelength of the knee varies from 40 m in Fig. 16 to about 300 m in the examples given by Villain *et al.* (1986). Thus, from the results of both DE-2 and A-3, one obtains a complete image of the electric field and density spectra in the gradient drift turbulence: a power law spectrum with a spectral index of the order of 1.8 for long wavelengths, between 10 km and a variable lower limit; at smaller wavelengths, the slope increases to values of the order of 3. The wavelength of the transition between these two regimes varies from case to case, with a minimum value of 40 m. Such multi-slope power spectra have also been deduced from phase scintillation measurements by Fremouw *et al.* (1985).

Numerical simulations of interchange instabilities by Keskinen and Huba (1990), taking ionospheric-magnetospheric coupling into account, have shown that inertial effects modify the long-wavelength spectrum and that the instability remains purely collisional at small wavelengths. They find a transition wavelength of the order of 2–3 km (2.5–4 Hz) where the spectrum breaks, with a smaller slope at long wavelengths than at short wavelengths. This transition is below the long wavelengths studied by DE-2 and above those studied by A-3. Experimentally, if we consider the DE-2 and A-3 results together, it appears that there is no such break in the spectrum. However, as discussed above, a strong break in the spectrum if often observed, but at much shorter wavelengths, of the order of 40 m. Furthermore, the simulations made by Keskinen and Ossakow (1983 b) for the wavelength range of A-3 have given spectral indices of 2.4–2.5 for the electron density which are significantly larger than the 1.6–1.8 experimental value given by Fig. 8.

A-3 results show that the spectral indices of the electric field in shear-driven turbulence are larger than those measured in gradient-drift turbulence. From DE-2 results (paper 1), it is shown that the mean electric field spectral index is 1.8 in strong shears, but that it increases to 3.0 in moderate shears. This is in agreement with the examples shown on Fig. 14. It could also explain the fairly large spread of the indices shown by the histograms of Fig. 15, in which we have considered all shears, regardless of their intensity.

Keskinen *et al.* (1988) have performed numerical simulations of the Kelvin-Helmholtz instability with a sheared flow perpendicular to the ambient magnetic field. They found that, regardless of the intensity of the shear, the spectral indices of the density and electric field depend upon two parameters: (1) the importance of the Pedersen coupling; (2) the direction along which the turbulent spectrum is measured, either parallel or perpendicular to the shear direction. Numerically, their results show that the spectral index of the electric field (assumed to be two units less than that of the electric potential) varies from 3.4 in the absence of Pedersen coupling to 2.6 or 3.3 (according

to whether the spectrum is taken along or perpendicular to the shear direction) in the case of a Pedersen coupling characteristic of the auroral *F*-region. A certain discrepancy is noted between these simulations and A-3 results, since the simulation values are larger than the mean value measured by A-3 (Fig. 15, middle panel). More precisely, only 20% of the α_H values measured by A-3 belong to the above range, the remaining 80% being below 2.6.

Two-dimensional turbulence theory based on a narrow injection band of wave numbers ($k=k_i$) has been discussed by Kintner and Seyler (1985). For shear flow or magnetospherically-forced turbulence, they predict an inverse cascade regime with a $k^{-5/3}$ spectrum at long wavelengths ($k<k_i$) and a direct cascade with a sharper k^{-3} spectrum at small wavelengths ($k>k_i$). Such theoretical spectra can fit the experimental multi-slope spectra discussed above, although there is no evidence (direct or indirect) for an energy injection process at the wavelength of the knee.

Kelley (1989) suggested that the mixing of ionospheric density gradients by the magnetospheric turbulent convection flow pattern could be a source for small scale irregularities. He showed that the ratio between the linear growth rates of the turbulent mixing process and the gradient drift instability is equal to the ratio E_{rms}/E_0 of the turbulent to the DC electric fields. The relatively low experimental values of E_{rms} (typically 0.1 mV/m) suggests that turbulent mixing is not likely to be a strong source of turbulence in the frequency/wave-number range considered in this paper.

An important result of the present study is the large value of the magnetic field spectral indices (centered on 3.6), which are systematically larger than those of the electric field, leading to a ratio $\langle B^2\rangle/\langle E^2\rangle \sim k^{-1.8}$. Such a large difference between the spectral indices of electric and magnetic fluctuations has already been observed by Hawkeye (Kintner, 1976; Kintner and Seyler, 1985) and DE-1 (Gurnett *et al.*, 1984). It has been suggested by Forget *et al.* (1991) that this behaviour can be the signature of static structures of field aligned currents with a small transverse scale, through which the satellite is moving: due to the imperfect mapping of transverse electric fields between the magnetosphere and the lower ionosphere, the parallel currents with a small transverse scale tend to close horizontally at a higher altitude than those with a larger transverse scale. At these higher altitudes, the Pedersen conductivity is smaller, as well as the current and the magnetic field. This can explain why the magnetic power is observed to decrease with wavelength more rapidly than the electric power.

Ratio of electric to density fluctuations

In paper 2, it is shown that the ratio of the electric field to the density fluctuations is at least one order of magnitude larger in velocity shear driven turbulence compared to the value of the same ratio produced by the gradient drift instability. The average values deduced from A-3 measurements are summarized in Table 1, and compared with those deduced from DE-2 (paper 2, their Fig. 20). Our results essentially confirm those of DE-2. However, the mean value of the ratio $(E/(\Delta N/N)$ measured by A-3 in the gradient drift turbulence is smaller than that measured by DE-2, a difference which could be attributed to the different frequency ranges covered by the two experiments. It must be noted that the dispersion in the values of this ratio is large, both in DE-2 and in A-3 data. The two orbits studied in paper 2 give different results, suggesting that this ratio is not an absolute characteristic of the gradient-drift turbulence, but that it depends upon other parameters which vary from one orbit to the other. Also, the A-3 results show a large dispersion in the values of $E/(\Delta N/N)$. For illustration, from Fig. 6, we can deduce that, in the gradient-drift turbulence, this ratio varies between 2 and 30 mV/m during orbit 2314 and between 2 and 8 mV/m during orbit 2242.

Table 1. Ratio (in mV/m) of the electric field and relative-density fluctuations measured by Aureol-3 and DE-2. The values for DE-2 are deduced from Fig. 20 of Basu *et al.* (1990)

	Gradient-drift turbulence	Shear-driven turbulence
Aureol-3	7 (orbit 2314)	65 (at 20 Hz) 80 (at 100 Hz)
Aureol-3	4 (orbit 2242)	100 (at 20 Hz) 360 (at 100 Hz)
DE-2	15	180

In shear-driven turbulence, the $E/(\Delta N/N)$ ratio has been evaluated only in a limited number of cases. The values of this ratio (Table 1) are systematically larger than during the gradient-drift turbulence events, by one to two orders of magnitude.

In the linear theory of the gradient-drift instability, the $E/(\Delta N/N)$ ratio can be interpreted as giving the DC electric field in the frame of the neutrals. The values given in the left column of Table 1 appear fairly small in this context. In the numerical simulations of the gradient drift (Keskinen and Ossakow, 1983 b) and Kelvin-Helmholtz (Keskinen *et al.*, 1988) instabilities, no value of this ratio has been published. In the turbulent mixing theory of Kelley (1989), this ratio can take any value depending upon the intensity of the initial density gradient on which the mixing process is applied.

It must be remarked also that contrary to the DE-2 geometry where the electric fluctuation is the component along the spacecraft trajectory along which the density fluctuation is also measured, the E_H component measured by A-3 is close to transverse to the spacecraft trajectory. This may explain the differences noted above between the DE-2 and A-3 results, if the turbulence is not isotropic in the plane perpendicular to the Earth's magnetic field.

Conclusions

Electric and magnetic fields and electron density measurements made on board the Arcad-Aureol-3 satellite are used to study the small-scale turbulent structure of the

high-latitude topside ionosphere. The frequency range is between 12.5 and 200 Hz, which corresponds to spatial wavelengths between 40 m and 640 m. Two regions of turbulence have been identified: (1) the auroral zone, where the turbulence is most intense ($E=1$ mV/m rms) and is associated with precipitations, parallel currents and velocity shears; (2) the polar cap and sub-auroral zone, where the turbulence is less intense ($E=0.1$ mV/M rms) and associated with density gradients.

The most characteristic differences between these two types of turbulence are the observation of magnetic fluctuations in shear-associated turbulence and the value of the ratio of the electric field to the density fluctuations. This ratio is increased by a factor of 10 to 100 between the gradient-drift turbulence and the shear-associated turbulence.

Acknowledgements. The Aureol-3 spacecraft was launched in the frame of the ARCAD-3 program undertaken jointly by the Centre National d'Etudes Spatiales (CNES) in France and Intercosmos and the Space Research Institute (IKI) in the USSR. This study was supported through grants 80-81/CNES/224 and 88/CNES/1204. We thank J.J. Berthelier for helpful suggestions in the course of this work, and J.M. Bosqued for the permission to use the results of the SPECTRO experiment.

References

Basu, Su, Sa Basu, E. MacKenzie, P. F. Fougere, W. R. Coley, N. C. Maynard, J. D. Winningham, M. Sugiura, W. B. Hanson, and W. R. Hoegy, Simultaneous density and electric field fluctuation spectra associated with velocity shears in the auroral oval, *J. Geophys. Res.*, **93,** 115–136, 1988.

Basu, Su, Sa. Basu, E. MacKenzie, W. R. Coley, J. R. Sharber, and W. R. Hoegy, Plasma structuring by the gradient drift instability at high latitudes and comparison with velocity-shear driven processes, *J. Geophys. Res.*, **95,** 7799–7818, 1990.

Beghin, C., J.-F. Karczewski, B. Poirier, R. Debrie, and N. Massevitch, The Arcad-3 Isoprobe experiment for high time resolution thermal plasma measurements, *Ann. Geophys.*, **38,** 615–630, 1982.

Berthelier, J. J., F. Lefeuvre, M. M. Mogilevski, O. A. Molchanov, Yu. I. Galperin, J. F. Karczewski, R. Ney, G. Gogly, C. Guerin, M. Levêque, J. M. Moreau, and F. X. Sêné, Measurement of the VLF electric and magnetic components of waves and DC electric field on board the Aureol-3 satellite: the TBF-ONCH experiment, *Ann. Geophys.*, **38,** 643–668, 1982a.

Berthelier, J. J., A. Berthelier, Yu. I. Galperin, V. A. Gladyshev, G. Gogly, M. Godefroy, C. Guerin, and J. F. Karczewski, DC magnetic field observations on board the Aureol-3 satellite: the TRAC experiment, *Ann. Geophys.*, **38,** 635–642, 1982b.

Berthelier, J. J., C. Machard, J. C. Cerisier, A. Berthelier, and J. M. Bosqued, ULF electromagnetic turbulence in the high latitude ionosphere, *J. Geophys. Res.*, **93,** 5701–5712, 1988.

Cerisier, J. C., C. Beghin, and J. J. Berthelier, Unstable density gradients in the high latitude ionosphere, *Radio Sci.*, **20,** 755–761, 1985

Forget, B., J. C. Cerisier, A. Berthelier, and J. J. Berthelier, Ionospheric closure of small scale Birkeland currents, *J. Geophys. Res.*, **96,** 1843–1847, 1991.

Fredricks, R. W., and F. V. Coroniti, Ambiguities in the deduction of rest frame fluctuation spectra computed in a moving frame, *J. Geophys. Res.*, **81,** 5591–5595, 1976.

Fremouw, E. J, J. A. Secan, and J. M. Lansinger, Spectral behaviour of phase scintillation in the nighttime auroral region, *Radio Sci.*, **20,** 923–933, 1985.

Gurnett, D. A., R. L. Huff, J. D. Menietti, J. L. Burch, J. D. Winningham, and S. D. Shawhan, Correlated low frequency electric and magnetic noise along auroral field lines, *J. Geophys. Res.*, **89,** 8971–8985, 1984.

Holmgren, G., and P. M. Kintner, Experimental evidence of widespread regions of small scale plasma irregularities in the magnetosphere, *J. Geophys. Res.*, **95,** 6015–6023, 1990.

Huba, J. D., H. G. Mitchell, M. J. Keskinen, J. A. Fedder, P. Satyanarayana, and S. T. Zalezak, Simulations of plasma structure evolution in the high-latitude ionosphere, *Radio Sci.*, **23,** 503–512, 1988.

Kelley, M. C., *The earth's ionosphere, Plasma physics and electrodynamics,* International Geophysics Series, **Vol 43,** Academic Press, 1989.

Kelley, M. C., and F. S. Mozer, A satellite survey of vector electric field in the ionosphere at frequencies of 10 to 500 Hz, 1, Isotropic high latitude emissions, *J. Geophys. Res.*, **77,** 4158–4173, 1972.

Kelley, M. C., J. F. Vickrey, C. W. Carlson, and R. Torbert, On the origin and spatial extent of high latitude F region irregularities, *J. Geophys. Res.*, **87,** 4469–4475, 1982.

Keskinen, M. J., and J. D. Huba, Nonlinear evolution of high-latitude ionospheric interchange instabilities with scale-size dependent magnetospheric coupling, *J. Geophys. Res.*, **95,** 15157–15166, 1990.

Keskinen, M. J., and S. L. Ossakow, Non-linear evolution of plasma enhancements in the auroral ionosphere, 1-Long wavelength irregularities, *J. Geophys. Res.*, **87,** 144–150, 1982.

Keskinen, M. J., and S. L. Ossakow, Theories of high-latitude ionospheric irregularities: a review, *Radio Sci.*, **18,** 1077–1091, 1983a.

Keskinen, M. J., and S. L. Ossakow, Non-linear evolution of convecting plasma enhancements in the auroral ionosphere, 2-Small-scale irregularities. *J. Geophys. Res.*, **88,** 474–482, 1983b.

Keskinen, M. J., H. G. Mitchell, J. A. Fedder, P. Satyanarayana, S. T. Zalezak, and J. D. Huba, Nonlinear evolution of the Kelvin-Helmholtz instability in the high-latitude ionosphere, *J. Geophys. Res.*, **93,** 137–152, 1988.

Kintner, P. M., Observation of velocity shear turbulence, *J. Geophys. Res.*, **81,** 5114–5122, 1976.

Kintner, P. M., and C. E. Seyler, The status of observations and theory of high latitude ionospheric and magnetospheric plasma turbulence, *Space Science Reviews,* **41,** 91–129, 1985.

Mounir, H., *Turbulence électrostatique dans l'ionosphère à haute latitude,* Ph.D. thesis, Paris VI University, 1989.

Sugiura, M., N. C. Maynard, W. H. Farthing, J. P. Heppner, and B. G. Ledley, Initial results on the correlation between the magnetic and electric fields observed from the DE-2 satellite in the field-aligned current regions, *Geophys. Res. Lett.*, **9,** 985–988, 1982.

Temerin, M., The polarization, frequency and wavelength of high latitude turbulence, *J. Geophys. Res.*, **83,** 2609–2616, 1978.

Tsunoda, R. T., High-latitude F region irregularities: a review and synthesis, *Rev. Geophys.* **26(4),** 719–760, 1988.

Villain, J. P., C. Beghin, and C. Hanuise, Arcad3-Safari coordinated study of auroral and polar F region ionospheric irregularities, *Ann. Geophys.*, **4,** 61–68, 1986.